Hydrol. Earth Syst. Sci. Discuss., 9, 983–1011, 2012
www.hydrol-earth-syst-sci-discuss.net/9/983/2012/
doi:10.5194/hessd-9-983-2012

Hydrology and Earth System Sciences Discussions

Application of time domain induced polarization to the mapping of lithotypes in a landfill site

A. Gazoty[1], **G. Fiandaca**[1,2], **J. Pedersen**[1], **E. Auken**[1], **A. V. Christiansen**[1,3], **and J. K. Pedersen**[4]

[1]HydroGeophysics Group, Aarhus University, Denmark
[2]Department of Mathematics and Informatics, University of Palermo, Italy
[3]Geological survey of Denmark and Greenland (GEUS), Aarhus, Denmark
[4]Region Syddanmark, Vejle, Denmark

Received: 15 November 2011 – Accepted: 6 December 2011 – Published: 18 January 2012

Correspondence to: A. Gazoty (aurelie.legaz@geo.au.dk)

Published by Copernicus Publications on behalf of the European Geosciences Union.

Abstract

A DC resistivity (DC) and Time Domain Induced Polarization (TDIP) survey was undertaken at a decommissioned landfill site situated in Hørløkke, Denmark, for the purpose of mapping the waste deposits and to discriminate important geological units that control the hydrology of the surrounding area. It is known that both waste deposits and clay have clear signatures in TDIP data, making possible to enhance the resolution of geological structures, when compared to DC surveys alone.

Four DC/TDIP profiles were carried out crossing the landfill and another seven profiles in the surroundings, giving a dense coverage over the entire area. The whole dataset was inverted using a 1-D Laterally Constrained Inversion scheme, recently implemented for IP data, in order to use the entire decay curves for reconstructing the electrical parameters of the soil in terms of the Cole-Cole polarization model.

Results show that it is possible to both resolve the geometry of the buried waste body and key geological structures. In particular, it was possible to find a silt/clay lens at depth, which correlates with the flow direction of the pollution plume spreading out from the landfill, and to map a shallow sandy layer rich in clay that likely has a strong influence on the hydrology of the site. This interpretation of the geophysical findings was constrained by boreholes data, in terms of geology and gamma ray logging. The results of this study are important for the impact that the resolved geological units have in the hydrology of the area, making it possible to construct more realistic scenarios of the variation of the pollution plume as a function of the climate change.

1 Introduction

Due to the expected climate changes, there is an increasing need to develop geological models for predicting water flows in sensitive areas, such as former landfills. Indeed, it is believed that groundwater fluctuations will become more extreme in the years to come. As a consequence, it would affect the time pattern and the intensity of

HESSD
9, 983–1011, 2012

precipitation, yielding dry summers and more rainfall in the winter season in northern Europe (see some examples of scenarios in United Kingdom in Jackson et al., 2011; Hulme et al., 2002). At some places where aquifers are strongly influenced by surface water, this can lead to increased groundwater recharge and to a rising groundwater table. In Denmark, many landfills operational between 1950 to 1980 were designed without any kind of capture system underneath, leading to percolation through the waste and into the underlying geological layers and aquifer systems. In these cases, the predicted changes in winter rainfall will probably increase the risk of leaching of contaminants, which would, in turn, increase the outwash of chemical components from landfills to nearby aquifers. Landfills without leachate collection systems thus provide a high risk to future groundwater quality due to changes in groundwater level. In the light of these potential implications, it is important to have a fast, cheap and reliable technique which is able to depict the sub-surface at high resolution, both in landfill areas and surroundings, and, if present, gain information on pollution patterns. Such a technique involves the capability of characterizing waste deposits, but also the mapping and identification of different geological units. Direct Current resistivity (DC) and Time Domain Induced Polarization (TDIP or IP) have shown a good complementarity in that respect. It is known that the conductivity of porous rocks varies with their water content, ion concentration, mobility and the volume and arrangement of the pores. The conductivity of rocks increases with the conductivity of their pore fluids, as well as higher saturation degree and fractional pore space. The surface conductivity becomes important for materials with very large inner rock surfaces, such as clays (Kruschwitz and Yaramanci, 2004). The specific electrical behaviour of clay is usually explained by the presence of an external layer of cations in the so-called Electrical Double Layer (EDL, see Revil and Glover, 1997; Revil and Leroy, 2004) at the surface of clay particles (platelets). The cations can easily move tangentially to the surface, and the resulting surface conductivity contributes, together with the water volume conductivity, to the total conductivity (Tabbagh and Cosenza, 2007). Geophysical surveys have shown that the contribution of the surface conductivity associated with clay minerals is often the

HESSD
9, 983–1011, 2012

dominant term in vadose and phreatic zones characterized by low mineralized waters (Worthington, 1982). The induced polarization method has been used increasingly in environmental investigations because IP measurements are very sensitive to the low frequency capacitive properties of rocks and soils (Chen et al., 2008). These properties are associated with diffusion-controlled polarization processes that occur at the mineral-fluid interface (Slater and Lesmes, 2002). The IP phenomenon is often observed in media with electrical resistivities typically lying between 50 and 100 Ωm (the most common values for soils, see Michot et al., 2003) and containing a significant but non-dominant clay phase (Tabbagh et al., 2009). Usually, DC resistivity and IP are used jointly in order to discriminate between materials displaying an identical signature in resistivity (e.g. brine and clay). Slater and Glaser (2003) showed from the results of crosshole electrical imaging performed on sandy sediments, that high-resolution IP measurements might be used to make a lithological description, allowing a differentiation between silt/clay and sands of different grain size. Kemna et al. (2004) used the IP method in crosshole surveys in order to make a lithological characterization and to detect hydrocarbons. They also show how IP can significantly improve the understanding of the engineering properties of the subsurface relative to resistivity imaging alone. Recently, Auken et al. (2011), Gazoty et al. (2011a, b) and Leroux et al. (2010) have shown how the combined use of DC-TDIP could be successfully applied to landfill mapping and characterization, as it usually depicts the waste layer with a relatively high chargeable unit.

This study aims at delineating and characterizing the decommissioned Hørløkke landfill and the waste body with high accuracy. It also shows how the joint application of DC resistivity, IP and gamma ray logging enables a lithological description of the global area to be constructed and depict different geological layers with variable clay content at high resolution.

HESSD
9, 983–1011, 2012

2 The Hørløkke area

In the CLIWAT project a test site has been selected for the study of a typical Danish landfill and the surrounding geology by geophysical methods, as input to improve the knowledge for further modelling studies of hydrogeology and climate change scenarios. The area of interest is a decommissioned landfill, active from 1968 to 1978. It is located in the vicinity of Vojens, in southern Denmark (Fig. 1a), and covers an approximate area of 10 000 m^2. The total amount of waste deposited is estimated to be 65 000 m^3 (Pedersen et al., 2009), mainly consisting of domestic waste and sludge from Vojens wastewater treatment plant. Because the site was uncontrolled from 1972, some chemical waste from a refrigerator factory has also been dumped, but the amount remains unclear. The landfill was established without any kind of membrane, leachate capture or isolation systems. All waste was dumped on the original terrain, yielding a hillock approximately 15 m high. As a result of percolation through the landfill, contamination has been detected below the landfill itself, and extending 500 m west as a deep contamination plume (50–60 m depth). At the landfill, the contamination is mainly composed of hydrocarbons, iron and inorganic compounds, as well as a small amount of percolating chlorinated compounds. Within the plume, the contamination is composed of a high concentration of volatile chlorinated compounds and inorganic parameters.

The Hørløkke landfill is located on a small outwash plain, and is located in a topographic low, the general geology consisting of gravel and sand deposits, with local interbedded moraine clay layers (Fig. 2). At the landfill itself, the top layer consists of a 2–3 m thick clay filling layer, which covers the approximately 6–8 m thick waste layer.

From a hydrological point of view, the sequence of sand layers (see Fig. 2) constitutes a regional aquifer below the landfill. The aquifer reaches 100 m thick in some places, and the water level is shallow, within 2–3 m depth. The area around the landfill has been pointed out as a special drinking water and extraction area for Vojens waterworks (Pedersen et al., 2009). The landfill lies just west of the watershed, which means there is no risk for drinking water with the current location. However, climate

HESSD
9, 983–1011, 2012

change could involve the shift of the watershed further east, so that the contamination from the Hørløkke area might influence the water capture zone of Vojens waterworks. This is why an initial hydrogeophysical characterization investigation is needed, as input to constrain the geological models, and predict the different likely scenarios with the highest accuracy.

3 Materials and methods

3.1 DC and TDIP

The TDIP method measures the voltage decay induced by the turn-off of an exciting current pulse (see Fig. 3) and uses the characteristics of the decay to study the induced polarization of the soil, also known as chargeability. The equipment used in the field is the same as used for DC measurements, and thus the set-up consists of potential and current electrodes equally distributed along a profile. Immediately after the current is turned on, an induced potential, V_i, raises across the potential electrodes. After a charge-up effect, the primary voltage, V_{DC}, is measured for the computation of the direct current resistivity (DC) just before the current is turned off.

When the current is turned off, the voltage drops to a secondary level, V_s, and then decays with time during the relaxation period. This decay curve is the target of the Time Domain IP method, because it is characteristic of the medium, in terms of initial magnitude, slope and relaxation time. The signal V_{IP} along the decay is usually integrated over n time windows, or gates, for the computation of the chargeability M, which is expressed as

$$M(t) = \frac{1}{V_{DC} \cdot [t_{i+1} - t_i]} \int_{t_i}^{t_{i+1}} V_{ip} \mathrm{d}t \quad (1)$$

Where V_{DC} [V] is the potential used for calculating the DC resistivity, V_{ip} is the intrinsic or secondary potential [mV], t_i and t_{i+1} are the open and close times [s] for the gate over which the signal is integrated.

HESSD
9, 983–1011, 2012

3.2 Inversion scheme for DC-IP data

The inversion scheme used in this study enables the spectral content of the chargeability phenomenon to be extracted from time domain measurements. This spectral information is contained in the time decays, and its description is obtained using the Cole-Cole model (Pelton et al., 1978). The Cole-Cole model includes the DC resistivity and parameters describing the frequency dependency (c, τ and M_0, see the section below for further explanation). For each profile the whole dataset was inverted following Fiandaca et al. (2011a), where the time domain forward response is computed via a Hankel transform of the frequency domain response for a layered medium. Then, inversion is carried out with a 1-D-LCI implementation (Auken et al., 2005), to retrieve the four Cole-Cole parameters, for each layer. In the 1-D-LCI inversion algorithm, the model is composed of a set of laterally constrained 1-D models aligned along a profile (Auken et al., 2005). In practice, the LCI algorithm works by dividing a profile into several individual 1-D models, with one dataset for each model. The model parameters of layer resistivities/chargeabilities and depths are tied together laterally by claiming identity between neighbouring parameters within a specified variance (Auken et al., 2002), as illustrated schematically in Fig. 4.

3.3 The Cole-Cole model

There are a number of existing microscopic models that try to explain the IP phenomenon, among which are the double layer (Leroy et al., 2008) and throat models (Titov et al., 2002). Despite this, the most popular IP model for field application remains the Cole-Cole model, developed by Cole and Cole (1941) for the description of complex permittivity behaviour. It is used by Pelton et al. (1978) to describe complex resistivity. In the time domain, Pelton et al. (1978) showed that the intrinsic chargeability

HESSD
9, 983–1011, 2012

curves for Cole-Cole models in homogeneous media can be described by

$$M(t) = M_0 \sum_{n=0}^{\infty} \frac{(-1)^n \left(\frac{t}{\tau}\right)^{nc}}{\Gamma(1+nc)} \quad (2)$$

where τ [s], c [dimensionless] and M_0 [mV/V] are the Cole-Cole decay parameters. M_0 is the magnitude of the chargeability taken at $t = 0$, τ a time constant that characterizes the decay and c a constant which controls the frequency dependence, and is bounded between the values of 0.0 and 1.0; Γ is the Gamma function. In terms of physical properties, M_0 describes the magnitude of the polarization effect, and τ the relaxation time, indicating, in the frequency domain, the position of the phase peak. Pelton et al. (1978) and Luo and Zhang (1998) showed that M_0 and τ depend on the quantity of polarizable elements and their size, respectively, whereas c depends on the size distribution of the polarizable elements (Vanhala, 1997; Luo and Zhang, 1998).

3.4 Boreholes-gamma ray logging

Since 1990, more than 25 boreholes with a depth of ca. 85 m have been established near the landfill site (Fig. 1b) by reverse air rotary drilling for the collection of water samples and for providing a thorough lithological description. Geophysical logging (natural gamma, induction, resistivity) has been performed in half of the boreholes before casing. Each borehole was equipped with 4–6 screens over the depth from approximately 10 to 80 m below surface. Subsequently, natural gamma logs have also been performed inside the PEH casing in three boreholes.

The gamma ray logging (hereafter referred to as gamma log) measures the natural gamma radiation emanating from a formation. The major natural radio-isotopic sources that contribute to the radiation are thorium, uranium and potassium (Kirsch, 2006). Although there is no fixed rule regarding the amount of radioactivity for a given rock, shales, clays and marls are generally several times more radioactive than clean sands, sandstones, limestones and dolomites. In a given area, the only relative radioactivity

HESSD
9, 983–1011, 2012

of the various rocks is of significance. The gamma log is extremely useful, especially for discriminate among the different lithologies, because of its high vertical resolution. Clays are usually sufficiently high in radioactivity because their cation exchange capacity (CEC) allows to adsorb uranium and thorium. As a consequence, they can generally be easily distinguished from the other rocks formation on a gamma log.

Such types of borehole information is extremely useful to validate the results from surface measurements. In this study, borehole descriptions were superimposed to the 2-D sections to check the consistency of the results, but no a priori information was integrated to the inversion.

4 The survey

The area was investigated with the collection of 11 IP/DC sections of 410 m, both on top of the landfill and in the surroundings, all with an electrode spacing of 5 m (Fig. 1b). The survey was performed using the gradient array (Dahlin and Zhou, 2006), which was implemented on a Syscal-Pro instrument (Iris Instruments). The on and off-time lengths for the time decay measurements were set to 4 s. The data were acquired using logarithmically spaced gates (Effersø et al., 1999) with approximately eight gates per decade, with a total of 20 gates. Four sections have been performed on the landfill itself, all exceeding the landfill boundaries in order to cover both areas of low signal and expected high signal. Six other profiles are located either at the edge of the landfill or within the contaminated area, and one profile was set up outside the contaminated area to infer whether any different signature in IP/DC could be detected.

HESSD
9, 983–1011, 2012

5 Results

5.1 Landfill mapping

The inversion results for the four sections crossing the landfill are presented in Fig. 5. Because of the relevance of the parameter M_0 for depicting landfill areas, as shown by Auken et al. (2011), it was chosen in this paragraph to show the results from this parameter only. Within the landfill area, the chargeability model can be divided into three layers. The first layer on top is 3 to 5 m thick, with a chargeability of roughly 10 mV/V. Underneath, the second layer of 10 m thick displays a high chargeability signal up to 500 mV/V. The third deep layer in the model has a rather uniform chargeability of 10–30 mV/V. When comparing the models with the borehole information, there is a good match between these sharp boundaries and the different geological units. The first layer of 10 mV/V in the topsoil agrees with a clay filling layer present in the boreholes. The third layer in the chargeability model more likely fits a sand layer (again the top boundaries of the geological units and the model are completely consistent between each other), which is responsible for the low chargeability signal from 20 to 50 mV/V only. The high chargeable unit in between, of several hundreds of mV/V at 5–10 m depth, is laterally bounded within the anticipated landfill. Its depth and thickness perfectly fit the waste body revealed by the borehole information. Although inverted separately and independently (without any spatial constraints), the information content provided by the four inverted sections is very consistent between each other. Note that the high chargeable features on either side of the landfill, going down to depth, are most likely due to some topographic effects, as explained by Fox et al. (1980), and are therefore of no consequence to the interpretation in this study.

Figure 6 shows 1-D models in chargeability M_0, from the inverted profiles P1, P11, P15 and P16, at two locations where they roughly cross each other (cf. stars in Fig. 1b). At each intersection, there is an excellent match between the sections, in terms of depth, thickness and signal magnitude. A clear distinctive unit reaching 500 mV/V enhances the waste layer at 10 m depth. These results agree with Auken et al. (2011),

HESSD
9, 983–1011, 2012

Leroux et al. (2010) or Carlson et al. (2001) who report a high chargeable unit related to the waste body.

Because of the dense coverage of data across the landfill area and such a good fit between all sections, it is possible to map and characterize the former landfill boundaries with a high accuracy, both in terms of thickness and lateral extent. Figure 7 shows gathered 2-D sections in M_0 crossing and bounding the landfill. It enhances a perfect agreement between crossing profiles, as well as a strong contrast in M_0 between the dump site and the close surrounding area (around 50 times higher). In order to clarify the extent of the waste layer, an isovolume rendering of chargeability encompassed between 100–500 mV/V was added to the sections by following the method in Pryet et al. (2011). This range of chargeability was chosen because this is the signal level characterizing the waste body, as seen in Fig. 6. The isovolume with high chargeability is 50 000 m^3 big, which is in the same range of the a priori knowledge of the waste dumped in the landfill (65 000 m^3, after Pedersen et al., 2009).

5.2 Soil type discrimination

We have seen in the previous section that the landfill mapping and characterization could be done with high accuracy by the induced polarization method. Several profiles were performed in addition outside the landfill area in order to improve the geological description and clarify the presence of some specific patterns such as potential clay lenses, both in the shallow and deeper parts. Indeed, from Fig. 2 it appears that some clay layers are expected at 50–60 m depth, but the exact location in terms of depth and lateral extent remains unclear. It is, however, very important to gain knowledge of the geological description in order to improve the hydrogeological models and understand the flow pattern of the pollution plume. Care was taken to place the profiles on top of boreholes where possible, in order to correlate the information content provided by both methods. Results from profile 4 are presented in Fig. 8 with superimposed boreholes, for resistivity and chargeability. This profile is representative of the main resistivity/chargeability features present in the other profiles carried out in the

HESSD
9, 983–1011, 2012

landfill surroundings, and the geological interpretation of the geophysical inversions is presented in the next paragraphs.

5.2.1 Creek aquitard

In profile 4, within 150–200 m from the north, a shallow conductive lens of about 60 Ω m is present at 5–10 m depth (Fig. 8a). This lens is seen as a high chargeable layer of 80 mV/V in chargeability (Fig. 8b), and perfectly fits the clay-till layer (in brown) revealed by boreholes 151.1605, 151.1587 and 151.1477. Figure 9 shows a comparison between gamma logs performed in boreholes 151.1618, 151.1605, 151.1587 and 151.1477, and 1-D models of resistivity and chargeability fitting the same locations as boreholes (note that borehole 151.1477 is not consistent with the other three, but the gamma log experiment was carried out many years after the drilling, with the casing inside. For this reason the gamma log curve is not reliable). Within 5–10 m depth, Fig. 9a shows the good fit between the IP signal (high signal magnitude) and the gamma log, which displays a high peak signal of 40 cps. In addition, Fig. 9b shows that a low resistive layer is present at this depth, which is anti-correlated with the gamma log. The concordance of low resistivity/high chargeability with a high gamma log reinforces the presence of a clay layer without ambiguity. The dense coverage in IP/DC enables to define the lateral extent of this lens, observed from profiles 16 to 6 (not shown here). Again, there is a good match in resistivity and chargeability where the 2-D sections cross each other (e.g. between profiles 4 and 11). This clay layer underlies the Billund creek, which runs just north of the borders of the landfill, in the East-West direction. Thus, this layer is probably an aquitard, acting as a bed of low permeability along the aquifer.

5.2.2 Clay rich sandy layer

A moderately chargeable anomaly of less than 100 mV/V is present in the M_0 section of profile 4 at 20–40 m depth. This anomaly cannot be explained by the geological

HESSD
9, 983–1011, 2012

description of the boreholes, which report the soil at this depth only in terms of sand. However, the signal level is present with different extents in all the other profiles of the survey. As a matter of fact, purely sandy soil usually does not show high chargeability, and consequently, no high values for M_0. Between 20 and 40 m depth, Fig. 9a shows a high chargeable layer fitting a high gamma log for boreholes 151.1605 and 151.1587. At this depth, Fig. 9b shows a high resistive content contrary to the shallow part which is conductive. High gamma log and high chargeability usually indicate a significant clay content, but the resistivity method allows in this case to make the difference between a pure clay layer, which is expected to be conductive (as observed shallower, see paragraph above), and a clay rich sandy layer, which is more resistive, as found between 20 and 40 m depth. This example demonstrates the complementarity of IP, DC resistivity and gamma log, as the joint application of these three methods allows a detailed recognition of the different geological formations.

5.2.3 Deep silt/clay lens

Within 125–200 m from the north, profile 4 in Fig. 8 shows a more conductive feature at depth, reaching the basis of the section. This conductive bulk can be also observed in the raw data. Considering a 400 m profile with a 5 m takeouts, the depth of the feature remains on the ability of the DC method. This body can be considered as a true and reliable pattern, even though it is located at depth. In addition a conductive deep anomaly is present in all the other profiles going to the west, except profile 7. Figure 10 shows a 3-D plot of the resistivity models for all sections, with an isovolume in resistivity lower than 100 Ω m. This isovolume enhances a pattern which is near surface in the vicinity of the landfill, goes deeper in the west direction and stops before profile 7. Overall, the shape of this body has an extent of roughly 350 m, and, at some places, a width of 120 m. The deeper part of this conductive anomaly fits well with silt/clay content in boreholes, as also shown in Fig. 8.

HESSD
9, 983–1011, 2012

6 Discussion and conclusions

The geophysical survey, together with the borehole information, allowed the recognition and spatial delineation of several geological units important for the hydrology of the area. In particular it was possible to map three key structures that influence the water flow of the site: the clay layer that support the Billund creek north of the landfill; a clay-rich sandy layer at a depth of 20–40 m, that likely exhibits a different hydraulic conductivity when compared to the upper and lower clay-poor sandy soil; a silt/clay lens at depth, that extends about 350 m west from the landfill and that likely supports the flow of pollution in a westerly direction. A qualitative sketch of the survey findings that summarize these geological units is presented in Fig. 11. The use of both DC and TDIP data, instead of DC measurements alone, greatly enhanced the resolution power of the survey not only for the landfill delineation, but also for the characterization of the creek aquitard and for the recognition of the clay-rich sandy layer. In particular this last finding is noticeable, because the DC data alone did not show any evidence of the enriched clay content. These results are a perfect example of the potential of the IP method for hydrogeological studies and in landfill delineation, but more care is necessary in the field to obtain a good data quality in comparison with the acquisition of DC data only. The quality of the inverted sections presented in this paper can be attested by the perfect match between all information provided by the 2-D sections wherever they cross each other, even though each single section was inverted individually, without any spatial constraints. More importantly, the borehole information also allowed the outputs of the geophysical survey to be verified, the match between the two being excellent both inside and outside the landfill. The boreholes were also essential for the interpretation of the geophysical results, mainly for the clay-rich sandy layer and the silt/clay lens at depth. In our experience, the new inversion scheme adopted for inverting the data also played a significant role in the success of the interpretation of TDIP data. The detailed geological knowledge gained with the geophysical survey is particularly important in the investigated area, where the presence of the landfill

HESSD
9, 983–1011, 2012

and the related pollution plume provide a high risk for the underlying aquifer. More realistic scenarios of the variation of the outwash of chemical components from landfills to nearby aquifers, as a consequence of the climate change, will be predicted when incorporating such kind of information in the hydrogeological modelling.

Acknowledgements. This article is an outcome of the EU Interreg IVB project CLIWAT. It has been co-funded by the North Sea Region Programme 2007-2013 under the ERDF of the European Union.

References

Auken, E., Foged, N., and Sørensen, K. I.: Model recognition by 1-D laterally constrained inversion of resistivity data, in: Proceedings 8th meeting EEGS-ES, Aveiro, Portugal, 8–12 September 2002.

Auken, E., Christiansen, A. V., Jacobsen, B. H., Foged, N., and Sørensen, K. I.: Piecewise 1D Laterally Constrained Inversion of resistivity data, Geophys. Prospect., 53, 497–506, 2005.

Auken, E., Gazoty, A., Fiandaca, G., Pedersen, J., and Christiansen, A. V.: Mapping of Landfills using Time-domain Spectral Induced Polarization Data – The Eskelund Case Study, 17th European Meeting of Environmental and Engineering Geophysics (Near Surface), Leicester, UK, Expanded abstracts, E14, 12–14 September 2011.

Carlson, N. R., Hare, J. L., and Zonge, K. L.: Buried landfill delineation with induced polarization: progress and problems, in: Proceedings 14th meeting Symposium on the Application of Geophysics to Engineering and Environmental Problems (SAGEEP), Denver, Colorado, 4–7 March 2001.

Chen, J., Kemna, A., and Hubbard, S.S.: A comparison between Gauss-Newton and Markov-chain MonteCarlo-based methods for inverting spectral induced-polarization data for Cole-Cole parameters, Geophysics, 73, 247–258, 2008.

Cole, K. S. and Cole, R. H.: Dispersion and absorption in dielectrics, J. Chem. Phys., 9, 341–351, 1941.

Dahlin, T. and Zhou, B.: Multiple-gradient array measurements for multichannel 2D resistivity imaging, Near-Surface Geophysics, 4, 113–123, doi:10.3997/1873-0604.2005037, 2006.

HESSD

9, 983–1011, 2012

Effersø, F., Auken, E., and Sørensen, K. I.: Inversion of band-limited TEM responses, Geophys. Prospect., 47, 551–564, 1999.
Fiandaca, G., Auken, E., Christiansen, A. V., and Gazoty, A.: Full decay forward response modeling and direct inversion for Cole-Cole parameters, submitted to Geophysics on June 2011, 2011a.
Fiandaca, G., Auken, E., Gazoty, A., and Christiansen, A. V.: Full waveform modeling of time domain induced polarization data and inversion, Symposium on the Application of Geophysics to Engineering and Environmental Problems (SAGEEP), Charleston, South Carolina USA, 10–14 April 2011, SAGEEP 24 (140), doi:10.4133/1.3614087, 2011b.
Fox, C. R., Hohmann, G. W., Killpack, T. J., and Rijo, L.: Topographic effects in resistivity and induced polarization surveys, Geophysics, 45, 75–93, 1980.
Gazoty, A., Auken, E., Pedersen, J., Fiandaca, G., and Christiansen, A. V.: Reliability of Time domain Induced Polarization data, Symposium on the Application of Geophysics to Engineering and Environmental Problems (SAGEEP), Charleston, South Carolina USA, 10–14 April 2011, SAGEEP 24 (141), doi:10.4133/1.3614088, 2011a.
Gazoty, A., Fiandaca, G., Pedersen, J., Auken, E., and Christiansen, A. V.: Data repeatability and acquisition techniques for Time Domain Spectral Induced Polarization, Near Surf. Geophys., under review, 2011b.
Hulme, M., Jenkins, G. J., Lu, X., Turnpenny, J. R., Mitchell, T. D., Jones, R. G., Lowe, J., Murphy, J. M., Hassell, D., Boorman, P., McDonald, R. and Hill, S.: Climate change scenarios for the United Kingdom: the UKCIP02 scientific report, Tyndall Centre for Climate Change Research, University of East Anglia, Norwich, UK, 2002.
Jackson, C. R., Meister, R., and Prudhomme, C.: Modelling the effects of climate change and its uncertainty on UK Chalk groundwater resources from an ensemble of global climate model projections, J. Hydrol., 399, 12–28, doi:10.1016/j.jhydrol.2010.12.028, 2011.
Kemna, A., Binley, A., and Slater, L. D.: Crosshole induced polarization imaging for engineering and environmental applications, Geophysics, 69, 97–107, 2004.
Kirsch, R.: Groundwater geophysics – A Tool for Hydrogeology, Springer, 493 pp., ISBN 3-540-29383-3, 2006.
Kruschwitz, S. and Yaramanci, U.: Detection and characterization of the disturbed rock zone in claystone with the complex resistivity method, J. Appl. Geophys., 57, 63–79, 2004.
Leroux, V., Dahlin, T., and Rosqvist, H.: Time-domain IP and resistivity sections measured at four landfills with different contents, 16th Eurepean Meeting of Environmental and En-

HESSD
9, 983–1011, 2012

gineering Geophysics (Near Surface), Zürich, Switzerland, Expanded abstracts, P09, 6–8 September 2010.
Leroy, P., Revil, A., Kemna, A., Cosenza, P., and Ghorbani, A.: Complex conductivity of water-saturated packs of glass beads, J. Colloid Interf. Sci., 321, 103–117, doi:10.1016/j.jcis.2007.12.031, 2008.
Luo, Y. and Zhang, G.: Theory and Application of Spectral Induced Polarization, Geophysical Monograph Series No. 8, Society of Exploration Geophysicists, 171 pp., ISBN 1-56080-048-8, 1998.
Michot, D., Benderitter, Y., Dorigny, A., Nicoullaud, B., King, D., and Tabbagh, A.: Spatial and temporal monitoring of soil water content with an irrigated corn crop cover using surface electrical resistivity tomography, Water Resour. Res., 39, 1138, doi:10.1029/2002WR001581, 2003.
Pedersen, J. K., Christensen, J. F., Poulsen, A. R., Wernberg, T., and Jacobsen, O. K.: Nedbrydning af chlorerede opløsningsmidler I en dybtliggende forureningsfane vurderet på baggrund af vandanalyser og modellering, ATV Jord og Grundvand, 71–82, 2009.
Pelton, W. H., Ward, S. H., Hallof, P. G., Sill, W. R., and Nelson, P. H.: Mineral discrimination and removal of inductive coupling with multifrequency induced-polarization, Geophysics, 43, 588–609, 1978.
Pryet, A., Ramm, J., Chilès, J.-P., Auken, E., Deffontaines, B., and Violette, S.: 3D resistivity gridding of large AEM datasets: A step toward enhanced geological interpretation, J. Appl. Geophys., , 75, 277–283, doi:10.1016/j.jappgeo.2011.07.006, 2011.
Revil, A. and Glover, P. W. J.: Theory of ionic-surface conduction in porous media, Physical Review B, 55, 1757–1773, doi:10.1103/PhysRevB.55.1757, 1997.
Revil, A. and Leroy, P.: Constitutive equations for ionic transport in porous shales, Journal of Geophysical Research, 109, B03208, doi:10.1029/2003JB002755, 2004.
Slater, L. D. and Glaser, D. R.: Controls on induced polarization in sandy unconsolidated sediments and application to aquifer characterization, Geophysics, 68, 1547–1558, doi:10.1190/1.1620628, 2003.
Slater, L. D. and Lesmes, D.: IP interpretation in environmental investigations, Geophysics, 67, 77–88, doi:10.1190/1.1451353, 2002.
Tabbagh, A. and Cosenza, P.: Effect of microstructure on the electrical conductivity of clay-rich systems, Phys. Chem. Earth, 32, 154–160, doi:10.1016/j.pce.2006.02.045, 2007.
Tabbagh, A., Cosenza, P., Ghorbani,A., Guérin, R., and Florsch, N.: Modelling of Maxwell–

HESSD
9, 983–1011, 2012

Wagner induced polarisation amplitude for clayey materials, J./ Appl./ Geophys./, 67, 109–113, doi:10.1016/j.jappgeo.2008.10.002, 2009.
Titov, K., Komarov, V., Tarasov, V., and Levitski, A.: Theoretical and experimental study of time domain-induced polarization in water-saturated sand, J. Appl. Geophys., 50, 417–433, 2002.
Vanhala, H.: Mapping oil-contaminated sand and till with the spectral induced polarization (IP) method, Geophysical Prospecting, 45, 303–326, 1997.
Worthington, P. F.: The influence of shale effects upon the electrical resistivity of reservoir rocks, Geophys. Prospect., 30, 673–687, 1982.

HESSD
9, 983–1011, 2012

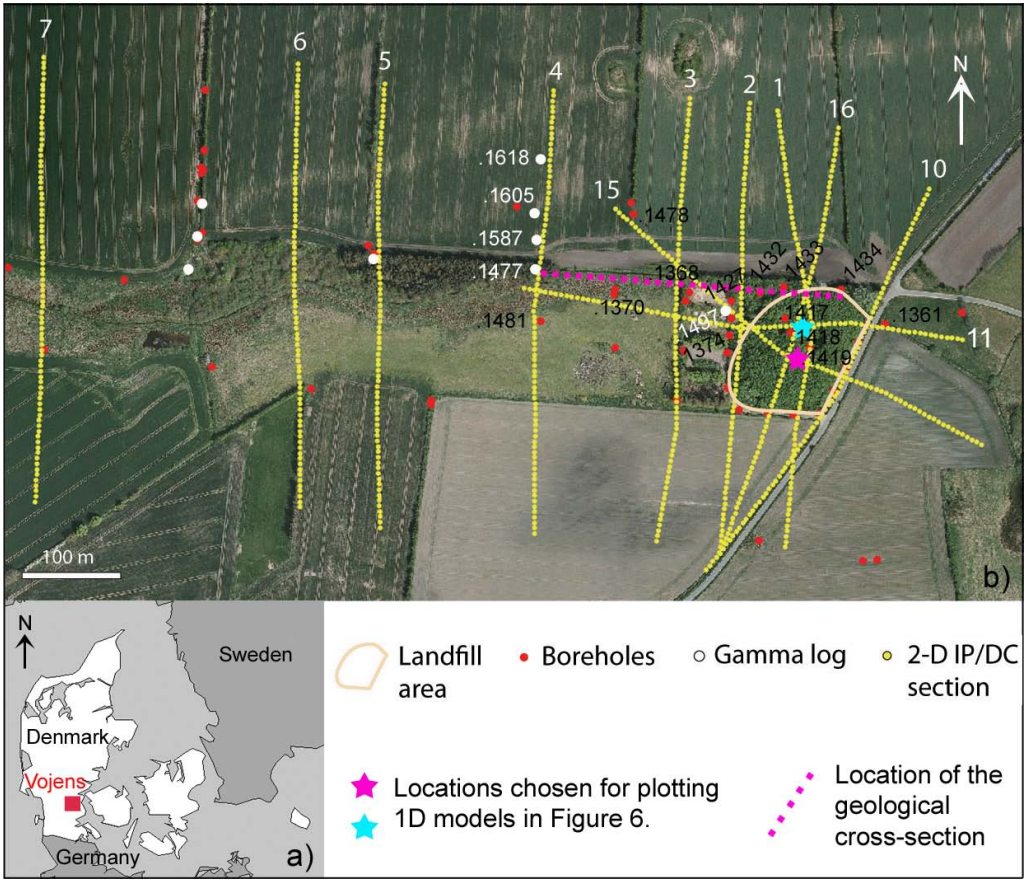

Fig. 1. The survey area. **(a)** Location of Vojens in the southern part of Denmark. **(b)** IP/DC sections (yellow dots) performed at the Hørløkke landfill (yellow area). The red dots point out the boreholes, the white dots refer to gamma log locations. The location of the watershed is outside the map. Copyright © Cowi.

HESSD
9, 983–1011, 2012

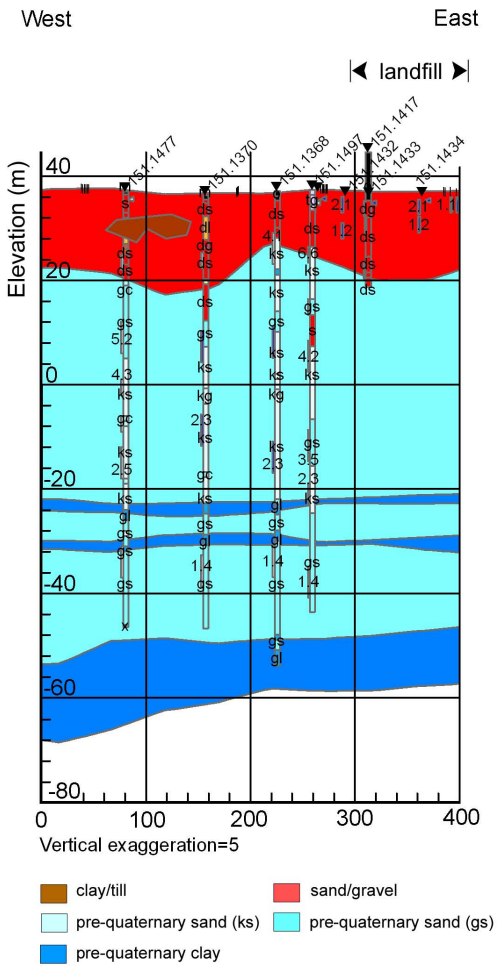

Fig. 2. Simplified geological cross-section (see location in Fig. 1). The glacial sands (shallow red layer) host a regional aquifer. Modified from Pedersen et al. (2009).

HESSD
9, 983–1011, 2012

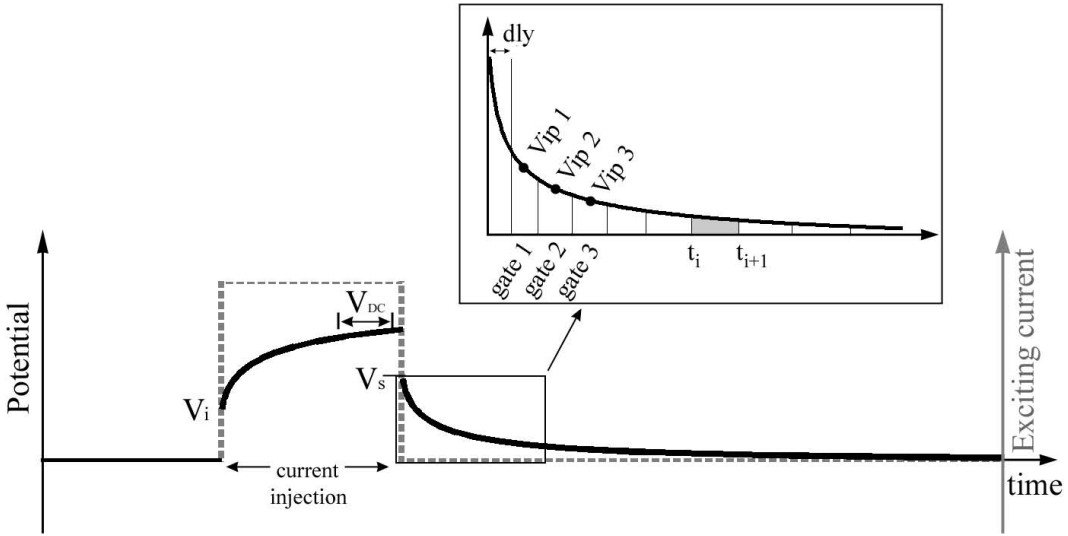

Fig. 3. Basic principles of Time Domain IP acquisition. The figure shows a sketch of the exciting current and the resulting voltage.

HESSD
9, 983–1011, 2012

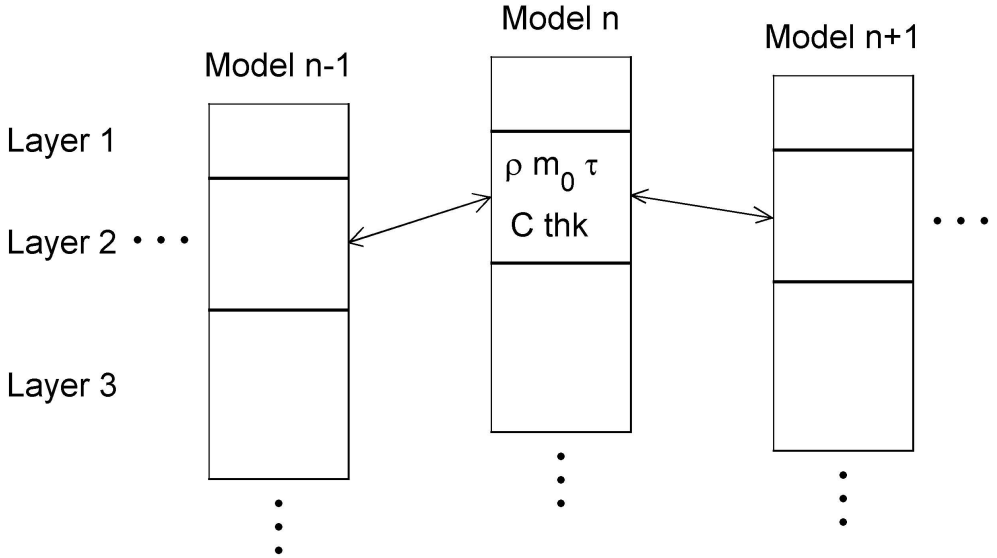

Fig. 4. Laterally Constrained Inversion (LCI) model set-up. The arrows represent the lateral constraints. From Fiandaca et al. (2011a).

HESSD
9, 983–1011, 2012

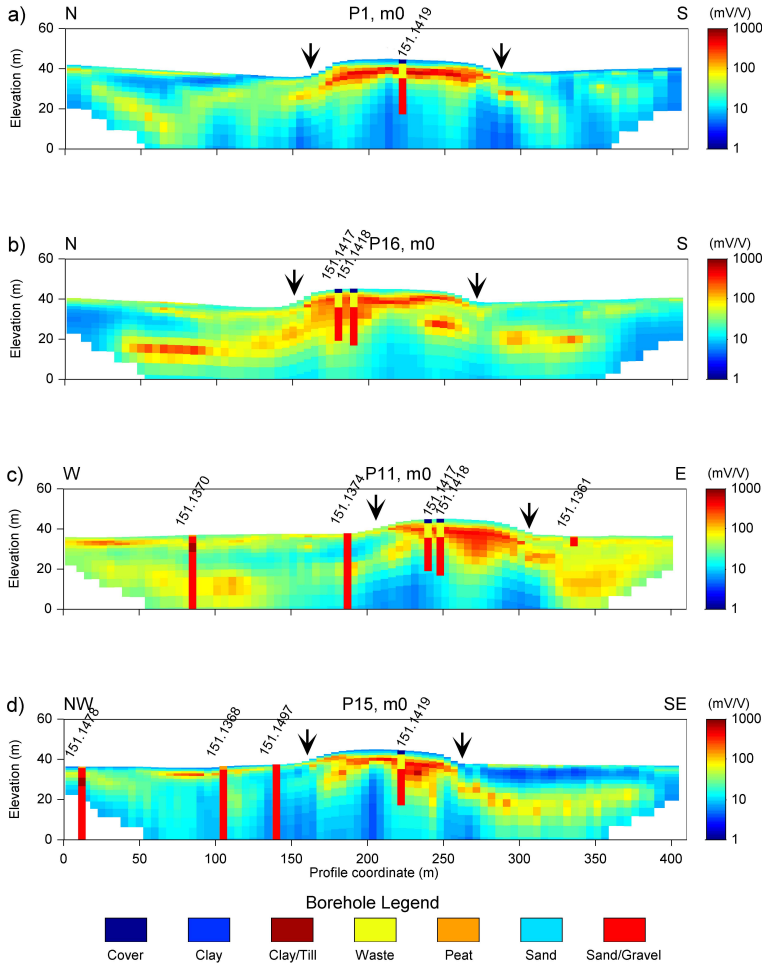

Fig. 5. Inverted sections in chargeability crossing the landfill with superimposed boreholes. The landfill is located within the arrows.

HESSD
9, 983–1011, 2012

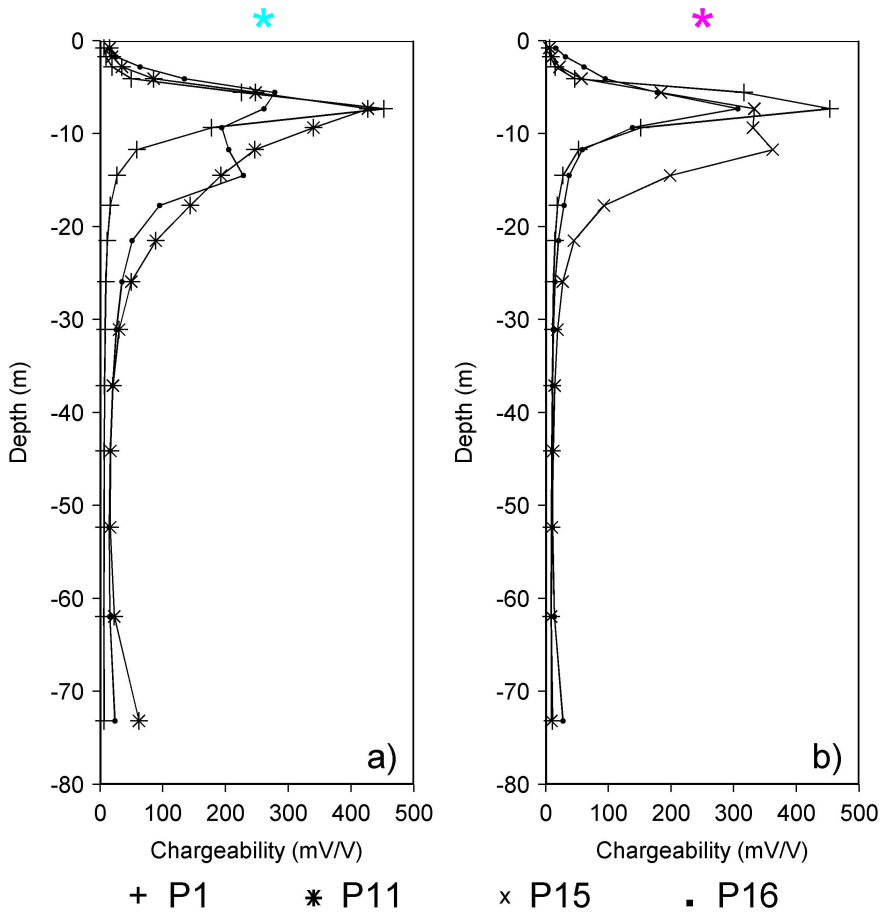

Fig. 6. Extracted models from the inverted surface measurements crossing the landfill. The stars refer to the locations on the map in Fig. 1. **(a)** 1-D models from profiles 1, 11 and 16. **(b)** 1-D models from profiles 1, 11 and 15.

HESSD
9, 983–1011, 2012

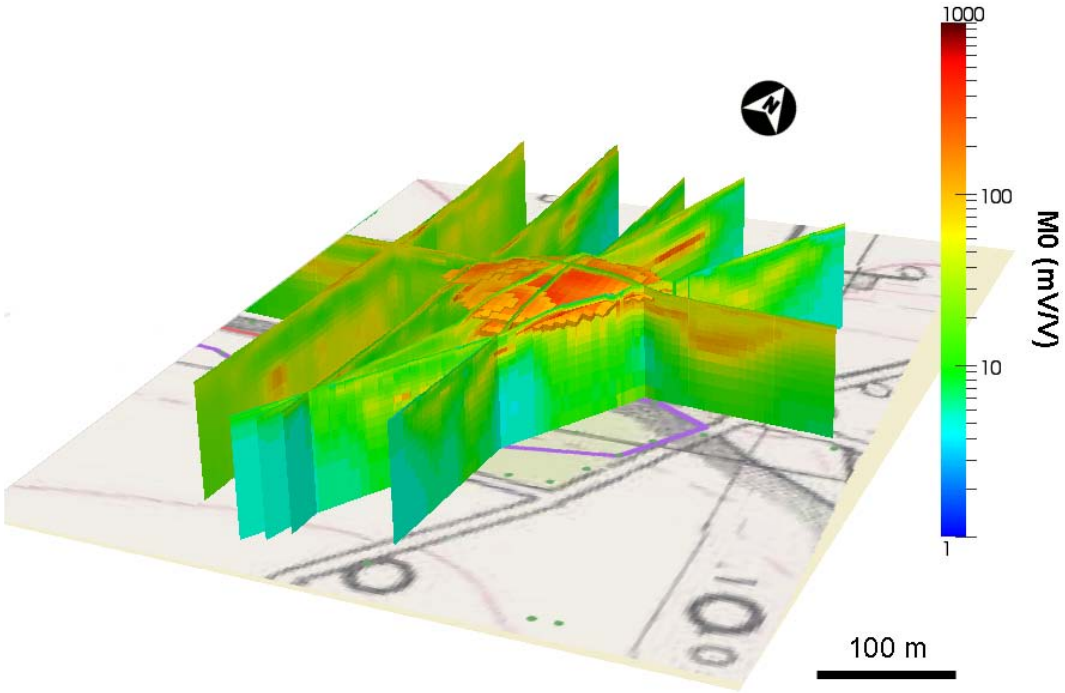

Fig. 7. 3-D chargeability plot of the Hørløkke landfill. The isovolume map with chargeability (M_0) above 100 mV/V allows to depict the landfill area without ambiguity.

HESSD
9, 983–1011, 2012

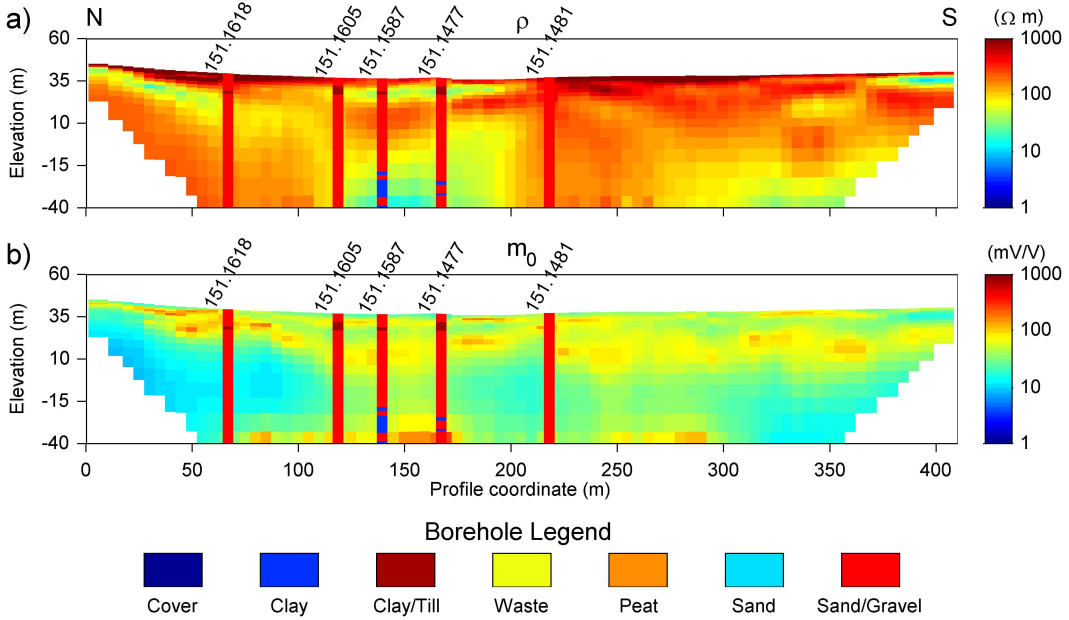

Fig. 8. Inverted sections for Profile 4 (see map in Fig. 1) with superimposed boreholes. **(a)** Resistivity section. **(b)** Chargeability M_0.

HESSD
9, 983–1011, 2012

Application of time domain induced polarization

A. Gazoty et al.

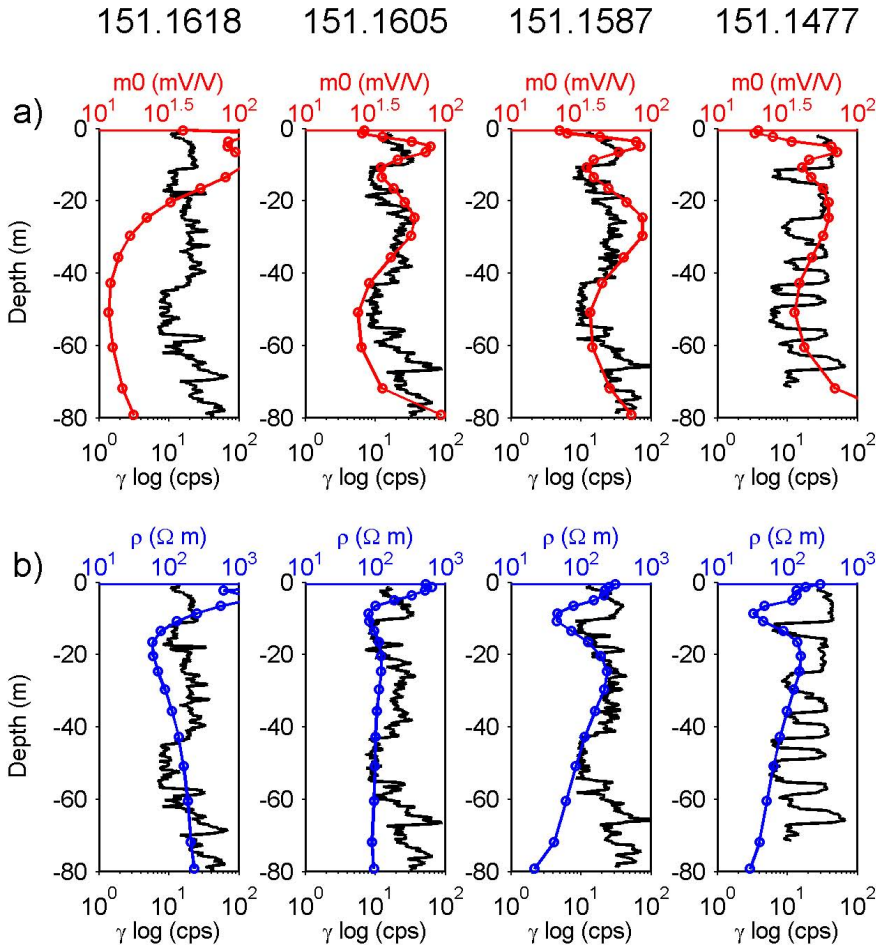

Fig. 9. Gamma logs (black) in comparison with 1-D models extracted from surface measurements. **(a)** Chargeability M_0. **(b)** Resistivity.

HESSD
9, 983–1011, 2012

Application of time domain induced polarization

A. Gazoty et al.

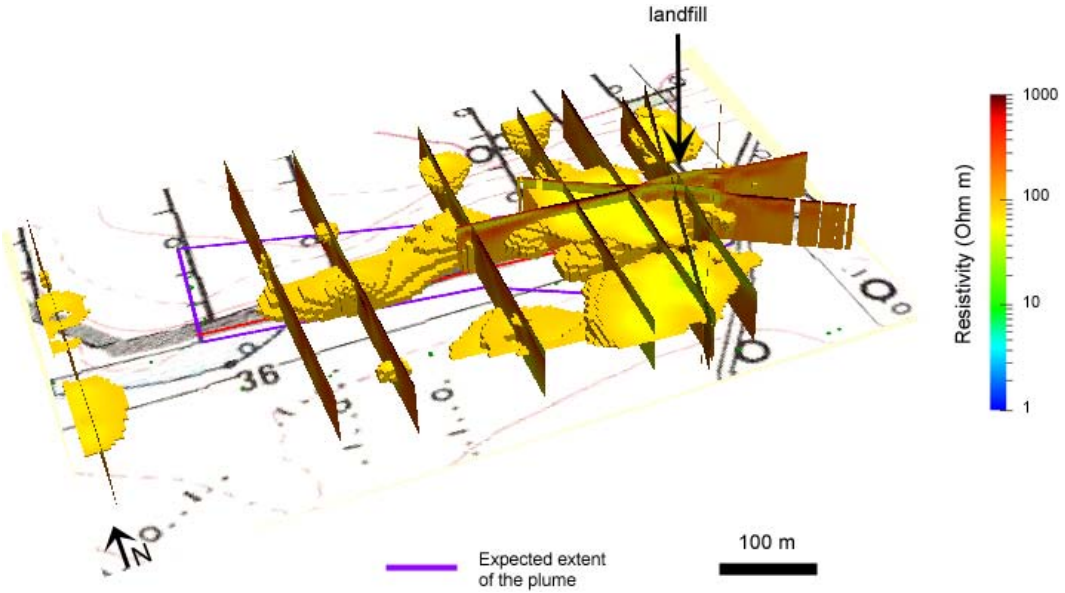

Fig. 10. Delineating the deep clay layer with the DC method: 3-D view of gathered resistivity sections with isovolume of resistivities lower than 100 Ωm. The anticipated extent of the plume is drawn in purple.

HESSD
9, 983–1011, 2012

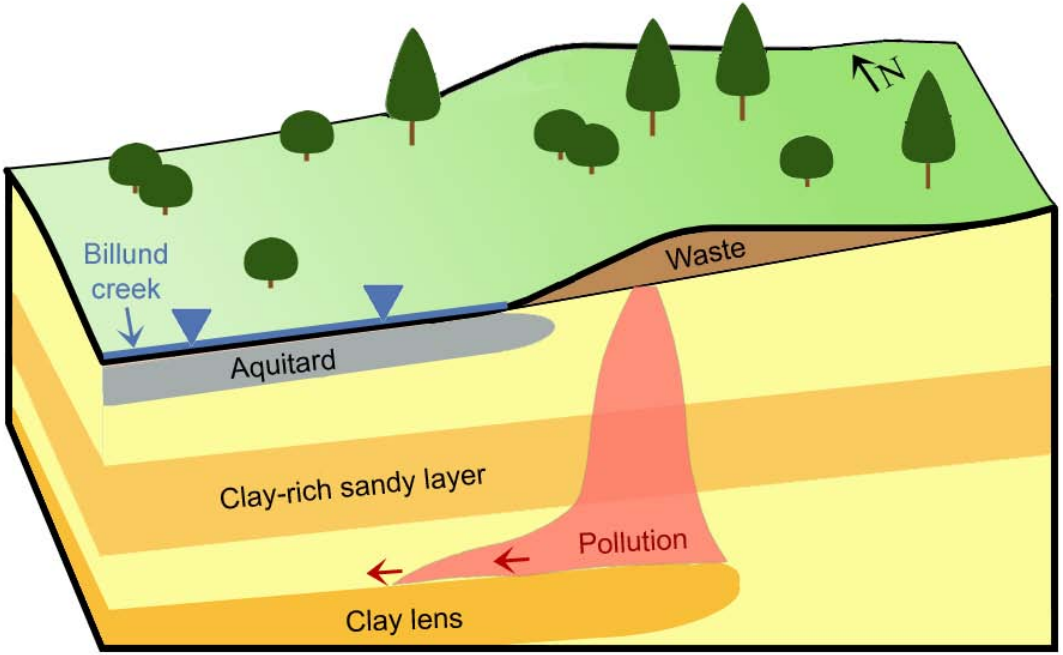

Fig. 11. Qualitative model obtained from geophysical measurements for a section crossing the landfill from West to East (not at scale).

HESSD
9, 983–1011, 2012